An Overview of BCC Climate System Model Development and Application for Climate Change Studies

WU Tongwen[1*] (吴统文), SONG Lianchun[1] (宋连春), LI Weiping[1] (李伟平), WANG Zaizhi[1] (王在志), ZHANG Hua[1] (张 华), XIN Xiaoge[1] (辛晓歌), ZHANG Yanwu[1] (张艳武), ZHANG Li[1] (张 莉), LI Jianglong[1] (李江龙), WU Fanghua[1] (吴方华), LIU Yiming[1] (刘一鸣), ZHANG Fang[1] (张 芳), SHI Xueli[1] (史学丽), CHU Min[1] (储 敏), ZHANG Jie[1] (张 洁), FANG Yongjie[1] (房永杰), WANG Fang[1] (汪 方), LU Yixiong[1] (路屹雄), LIU Xiangwen[1] (刘向文), WEI Min[2] (魏 敏), LIU Qianxia[1] (刘茜霞), ZHOU Wenyan[1] (周文艳), DONG Min[1] (董 敏), ZHAO Qigeng[1] (赵其庚), JI Jinjun[1] (季劲钧), Laurent LI[1,4], and ZHOU Mingyu[1,5] (周明煜)

1 *National Climate Center, China Meteorological Administration (CMA), Beijing* 100081*, China*

2 *National Meteorological Information Center, CMA, Beijing* 100081*, China*

3 *Institute of Atmospheric Physics, Chinese Academy of Sciences, Beijing* 100029*, China*

4 *Laboratoire de Météorologie Dynamique, Paris* 75005*, France*

5 *National Marine Environmental Forecasting Center, Beijing* 100081*, China*

(Received March 19, 2013; in final form November 15, 2013)

ABSTRACT

This paper reviews recent progress in the development of the Beijing Climate Center Climate System Model (BCC_CSM) and its four component models (atmosphere, land surface, ocean, and sea ice). Two recent versions are described: BCC_CSM1.1 with coarse resolution (approximately 2.8125°×2.8125°) and BCC_CSM1.1(m) with moderate resolution (approximately 1.125°×1.125°). Both versions are fully coupled climate-carbon cycle models that simulate the global terrestrial and oceanic carbon cycles and include dynamic vegetation. Both models well simulate the concentration and temporal evolution of atmospheric CO_2 during the 20th century with anthropogenic CO_2 emissions prescribed. Simulations using these two versions of the BCC_CSM model have been contributed to the Coupled Model Intercomparison Project phase five (CMIP5) in support of the Intergovernmental Panel on Climate Change (IPCC) Fifth Assessment Report (AR5). These simulations are available for use by both national and international communities for investigating global climate change and for future climate projections.

Simulations of the 20th century climate using BCC_CSM1.1 and BCC_CSM1.1(m) are presented and validated, with particular focus on the spatial pattern and seasonal evolution of precipitation and surface air temperature on global and continental scales. Simulations of climate during the last millennium and projections of climate change during the next century are also presented and discussed. Both BCC_CSM1.1 and BCC_CSM1.1(m) perform well when compared with other CMIP5 models. Preliminary analyses indicate that the higher resolution in BCC_CSM1.1(m) improves the simulation of mean climate relative to BCC_CSM1.1, particularly on regional scales.

Key words: Beijing Climate Center Climate System Model (BCC_CSM), atmospheric general circulation model, land surface model, oceanic general circulation model, sea ice model

Citation: Wu Tongwen, Song Lianchun, Li Weiping, et al., 2014: An overview of BCC climate system model development and application for climate change studies. *J. Meteor. Res.*, **28**(1), 034–056, doi: 10.1007/s13351-014-3041-7.

Supported by the National (Key) Basic Research and Development (973) Program of China (2010CB951902) and China Meteorological Administration Special Public Welfare Research Fund (GYHY201306020).

*Corresponding author: twwu@cma.gov.cn.

©The Chinese Meteorological Society and Springer-Verlag Berlin Heidelberg 2014

1. Introduction

Global climate and environmental changes under global warming are one of the great challenges facing human societies. These changes reflect the complex interactions among atmosphere, hydrosphere, lithosphere, cryosphere, and biosphere within the climate system. The development of theories and methodologies for investigating interactions and feedback mechanisms among the individual components of the climate system is a prerequisite to advanced understanding of the behavior of the climate system and to improved prediction of its future evolution. Climate system models are effective tools for objectively describing interactions in the climate system and exploring how these interactions impact climate change.

The National Climate Center (NCC) was established in 1995 under a national priority research project entitled "Research on Short-term Climate Prediction System in China". Under the auspices of the NCC, scientists from the China Meteorological Administration, Chinese Academy of Sciences, Ministry of Education, Ministry of Agriculture, and Ministry of Water Resources have together undertaken the research and development of a short-term climate prediction system. This collaborative work quickly yielded a first-generation atmospheric general circulation model (AGCM) (BCC_AGCM1.0; Dong, 2001), which was later followed by a coupled ocean-atmosphere model (BCC_CM1.0). This model system has played an important role in operational short-term climate prediction and studies of climate change in China (Ding et al., 2002, 2004, 2006; Zhang et al., 2004; Li et al., 2005; Luo et al., 2005; Zhao et al., 2005).

NCC initiated the research and development of a new-generation climate model system in 2005. This initiative has produced three second-generation versions of the AGCM (BCC_AGCM2.0, BCC_AGCM2.1, and BCC_AGCM2.2). NCC has also developed a first-generation land surface process model (BCC_AVIM1.0) that combines the vegetation dynamics and soil carbon cycle model AVIM developed by Ji (1995) with the Community Land Model version 3 (CLM3) developed at the National Center for Atmospheric Research (NCAR). The ocean model (MOM4_L40) has been modified from the Modular Ocean Model (MOM4) developed at the Geophysical Fluid Dynamics Laboratory (GFDL) to include the ocean carbon cycle. These component models serve as the basis for NCC's climate system model at coarse resolution (T42, or approximately 280 km; BCC_CSM1.1) and moderate resolution (T106, or approximately 110 km; BCC_CSM1.1(m)), in which the ocean, land surface, atmosphere, and sea ice components are fully coupled. This paper briefly reviews the development of these models and recent progress in their application to climate change studies.

2. Development of the BCC Climate System Model

2.1 Atmospheric General Circulation Model (AGCM)

2.1.1 BCC_AGCM2.0

BCC_AGCM2.0 is a spectral AGCM (Wu et al., 2008, 2010) with an adjustable horizontal resolution and 26 vertical layers. The default horizontal resolution is T42, which corresponds to approximately $2.8125°\times2.8125°$. This model is largely based on the NCAR CAM3 (Collins et al., 2004), but the reference atmosphere and surface pressure have been modified. The reference atmosphere represents the thermal structure of the mid/upper troposphere and stratosphere better than the default reference atmosphere used in CAM3 does. This modification reduces the effects of inhomogeneous vertical stratification and biases in topographic truncations, among other factors. Deviations in temperature and surface pressure from the reference atmosphere are treated as prognostic variables. Prognostic equations for water vapor, cloud water, cloud ice, and other hydrometeors are solved using a semi-Lagrangian approach. By contrast, the equations for vorticity, divergence, and deviations in temperature and surface pressure are solved using explicit or semi-implicit Eulerian methods. A detailed description of the dynamical framework has been provided by Wu et al. (2008). The model physics is mostly based on CAM3, with the following improvements. First, the parameterization scheme for mass-flux type cumulus convection developed by Zhang and McFarlane (1995) has been adapted as proposed by Wu et al. (2010). Second, a dry adiabatic adjustment scheme has been introduced to conserve potential temperature throughout the whole layer. Third, the parameterization of snow cover proposed by Wu and Wu (2004) has been adopted. Improved parameterizations of sensible and latent heat fluxes from the ocean surface that consider the effects of surface waves have been proposed (Wu et al., 2010). Land surface processes are simulated using the CLM3 (Oleson et al., 2004). The BCC_AGCM2.0 model has been shown to accurately simulate the current climate and annual cycle (Wu et al., 2010), decadal changes in precipitation in the East Asian and Asian/Australian monsoon regions (Wang et al., 2009; Chen et al., 2012), changes in the occurrence of extreme temperature and precipitation events (Chen et al., 2011; Dong et al., 2012), cloud radiative forcing (Guo et al., 2011), the Madden-Julian oscillation (Dong et al., 2009), the Meiyu season in the Yangtze-Huai River basin (Shen et al., 2011), and heavy precipitation processes in China (Jie et al., 2010).

Recently, Zhang Hua et al. (2012) coupled the BCC_AGCM2.0 with the CUACE Aerosol Model (BCC_AGCM2.0.1_CAM). CUACE is based on the Canadian Aerosol Module (CAM) (Gong et al., 2002, 2003) developed in collaboration with the Chinese Academy of Meteorological Sciences. CUACE is a particle size distribution model. It includes multi-cycle physical and chemical processes, such as the emission, transport, transformation, cloud interactions, and deposition of five common aerosol types (sulfate, black carbon, organic carbon, dust, and sea salt). Aerosol emission data were taken from a model intercomparison with aerosol observations (AeroCom; http://aerocom.met.no/aerocomhome.html), which includes gas-phase chemistry and provides an exploratory tool for simulating changes in aerosol distributions and assessing their implications for climate. Zhao et al. (2013) provided a preliminary evaluation of BCC_AGCM2.0.1_CAM simulations of the distributions and climatic impacts of these common aerosols. The model simulations of these aerosols generally agree well with observations. Zhang Hua et al. (2012) used BCC_AGCM2.0.1_CAM to simulate the global radiative forcing of three anthropogenic aerosols (black carbon, organic carbon, and sulfate) and two natural aerosols (dust and sea salt). Output from these simulations was included in the AeroCOM Phase II model intercomparison of aerosol radiative forcings (Myhre et al., 2012).

Several studies have used BCC_AGCM2.0 to examine parameterizations of cloud and radiation physics. Jing and Zhang (2012) applied a new Monte Carlo Independent Column Approximation-based (McICA) cloud-radiation framework within BCC_AGCM2.0. This framework provides a more flexible description of the sub-grid cloud structure. Their results show that perturbations to the model variables caused by McICA stochastic errors are small, with little impact on the model climate. Differences between global mean values and reference values calculated with the Independent Column Approximation (ICA) approach are within $\pm 0.01\%$, so the climate characteristics (including zonal, vertical, and sub-regional distributions) are largely consistent with ICA. The McICA cloud-radiation scheme used in BCC_AGCM2.0 has a higher confidence than the original scheme. Under McICA, radiation processes in the model have been updated to include the independently-developed BCC-RAD parameterization scheme. Greenhouse gas (GHG) concentrations are derived by using a K-distribution module (Zhang Hua et al., 2003, 2006a, 2006b; Shi and Zhang, 2007), while aerosol optical properties are calculated based on results reported by Wei and Zhang (2011) and Zhang Hua et al. (2012). BCC-RAD has participated in the AeroCom radiation model intercomparison. Cloud and radiation processes are independent under McICA. It is therefore relatively easy to adjust cloud structure and further improve the radiation model, with good prospects for the future development and application of BCC_AGCM.

2.1.2 BCC_AGCM2.1 and BCC_AGCM2.2

The most recent versions of BCC_AGCM2 are BCC_AGCM2.1 (with a T42 global resolution) and BCC_AGCM_2.2 (with a T106 global resolution, roughly corresponding to 110 km). These new versions include the following improvements. First, a new parameterization scheme for deep cumulus convections developed by Wu (2012) has been introduced. This scheme has been tested in a single column model configuration using data from Atmospheric Radiation Measurement (ARM) stations during the summers of 1995 and 1997. When used in combination with the Hack shallow convection scheme (Hack, 1994) and parameterizations of stratiform precipitation (Rasch and Kristjansson, 1998; Zhang Minghua et al., 2003), the Wu (2012) convection scheme successfully reproduces the intensity and evolution of major precipitation events. Second, parameters derived from cloud amount have been further optimized and improved. Third, an option for predicting global mean CO_2 concentrations has been added. Finally, the BCC_AVIM1.0 land surface model is now used to simulate land-atmosphere fluxes. BCC_AGCM2.1 and BCC_AGCM2.2 are the atmospheric components of the climate system models BCC_CSM1.1 and BCC_CSM1.1(m), respectively.

A set of standard atmospheric model intercomparison (AMIP) tests driven by observed forcing data (including sea surface temperature and the distribution of sea ice, solar activity, aerosols, and GHGs) have demonstrated the capabilities of BCC_AGCM2.1 and BCC_AGCM2.2 for simulating climate. Figure 1 shows interannual and decadal changes in global mean temperature anomalies over land during the period 1978–2006. Both models largely capture observed variations in temperature. Correlations with version 4 of the Climatic Research Unit (CRU) reconstructed temperature (Brohan et al., 2006) are 0.90 for BCC_AGCM2.1 and 0.87 for BCC_AGCM2.2. Both models also capture the observed spatial distributions of winter and summer precipitation during 1979–2008 (Fig. 2), although biases in summer precipitation are substantial in both models. These biases are particularly pronounced over eastern China, where the belt of strong precipitation is located further west than observed. Underestimates of summer precipitation are common to many internationally available climate models, and arise from multiple factors. Although these factors require more in-depth investigations, they may include errors in simulating land surface processes over the Tibetan Plateau or the location of the western Pacific subtropical high. The higher-resolution BCC_AGCM2.2 provides a better simulation of regional precipitation than BCC_AGCM2.1, along with better simulations of the centers of heavy precipitation over Southwest China, South China,

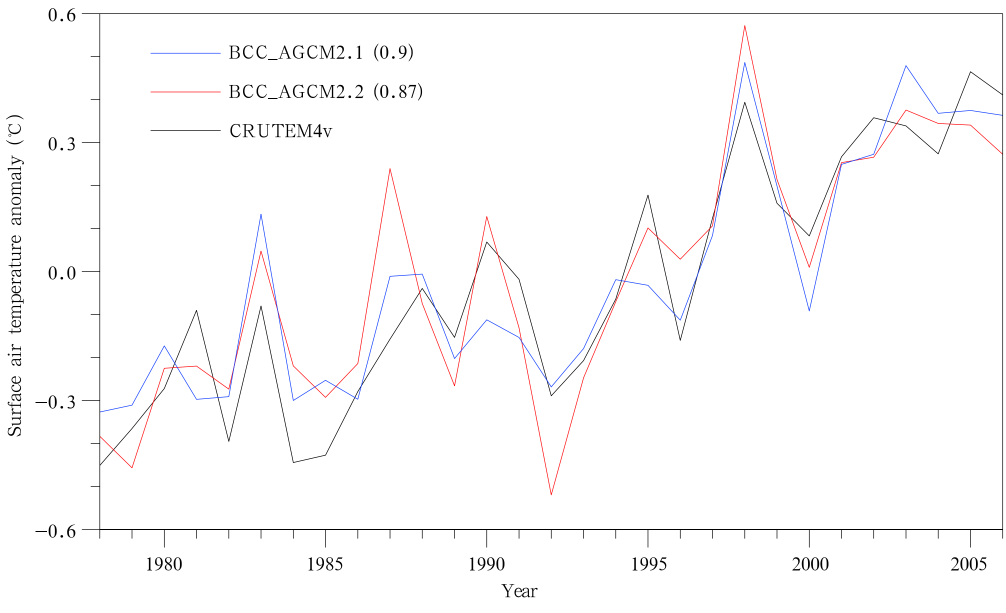

Fig. 1. Surface air temperature anomaly (°C) over global land areas from BCC_AGCM2.1, BCC_AGCM2.2, and CRUTEM version 4. Anomalies are calculated relative to the 1978–2006 mean. The correlations of the model time series relative to the observations are shown in brackets.

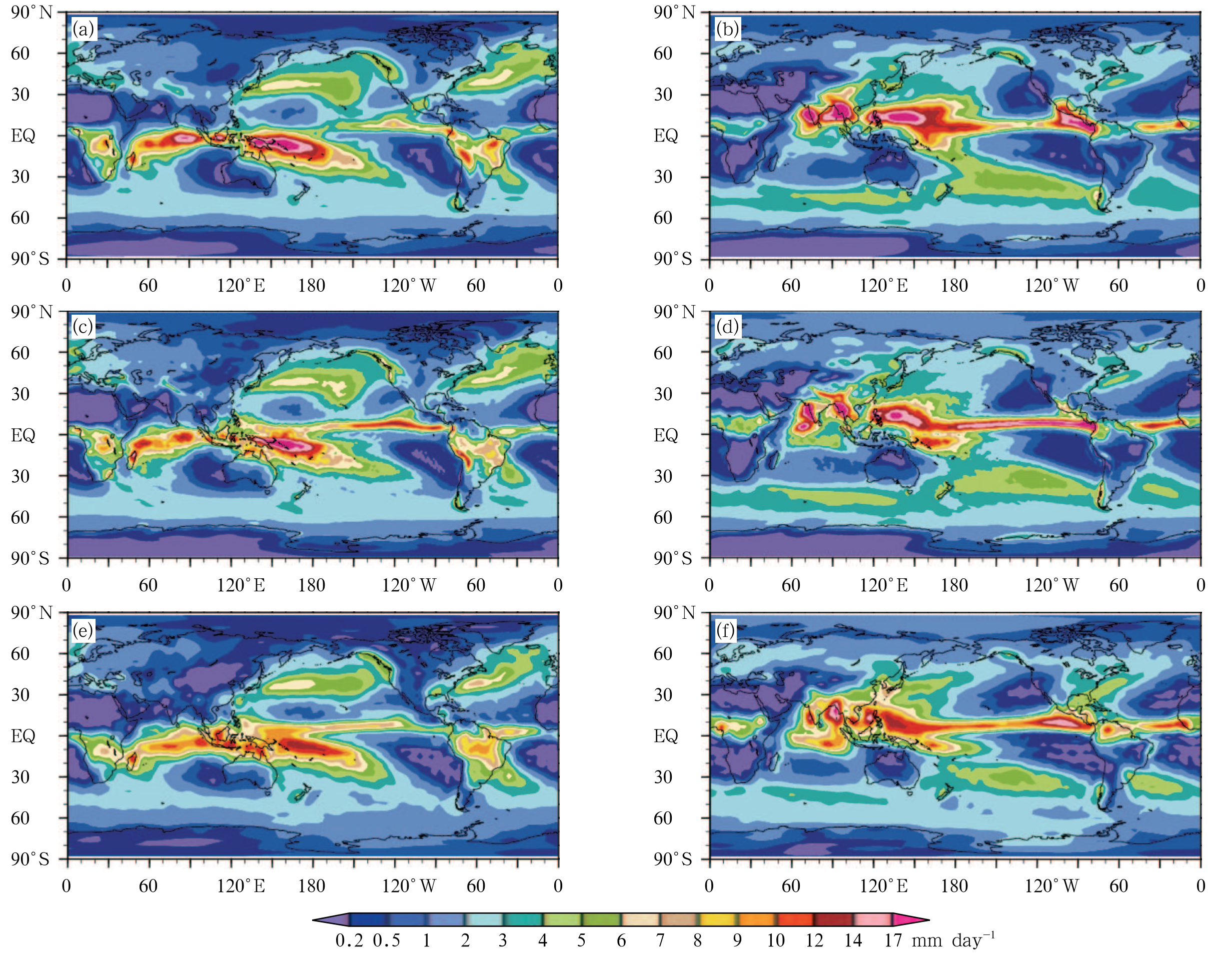

Fig. 2. Climatological mean precipitation (mm day^{-1}) for (a, c, e) DJF and (b, d, f) JJA from (a, b) BCC_AGCM2.1, (c, d) BCC_AGCM2.2, and (e, f) the reconstructed observation by Xie and Arkin (1997).

South Asia, and the Southeast Asian monsoon region.

Lu et al. (2014) analyzed an AMIP run of BCC_AGCM2.1 that covers the period 1979–2008. They reported that the model simulations of the zonal mean wind fields, temperature distributions, and seasonal variations in the stratosphere were consistent with those in the NCEP/NCAR reanalysis. The model was also able to simulate seasonal changes in the stratospheric polar vortex, although it generally underestimated temperatures both near the tropopause and in the upper stratosphere. Major biases in the simulated temperature profiles and upper-air jet streams relative to the reanalysis were mainly confined to wintertime mid and high latitudes. Lu et al. (2014) pointed out that these biases might be linked to perturbation processes in the model. Analysis of the Eliassen-Palm (E-P) flux (Figs. 3a–c) indicates that both equatorward and poleward propagations of planetary waves tend to be weaker when the model is weakly perturbed. When the equatorward propagation of planetary waves in the model is strong, most of the energy generated by the perturbation will be transported to lower latitudes. By contrast, the poleward propagation of planetary waves is relatively weak (short arrows in Figs. 3a–c). Perturbations reaching the middle and upper stratosphere are dominated by upward motion, which may lead to weaker poleward propagation in the vortex. These issues likely play a major role in the model overestimating of the strength of the polar vortex and underestimating of wintertime temperature in the Northern Hemisphere stratosphere. Analysis of the E-P flux divergence (Figs. 3d–f) shows a zone of strong E-P flux

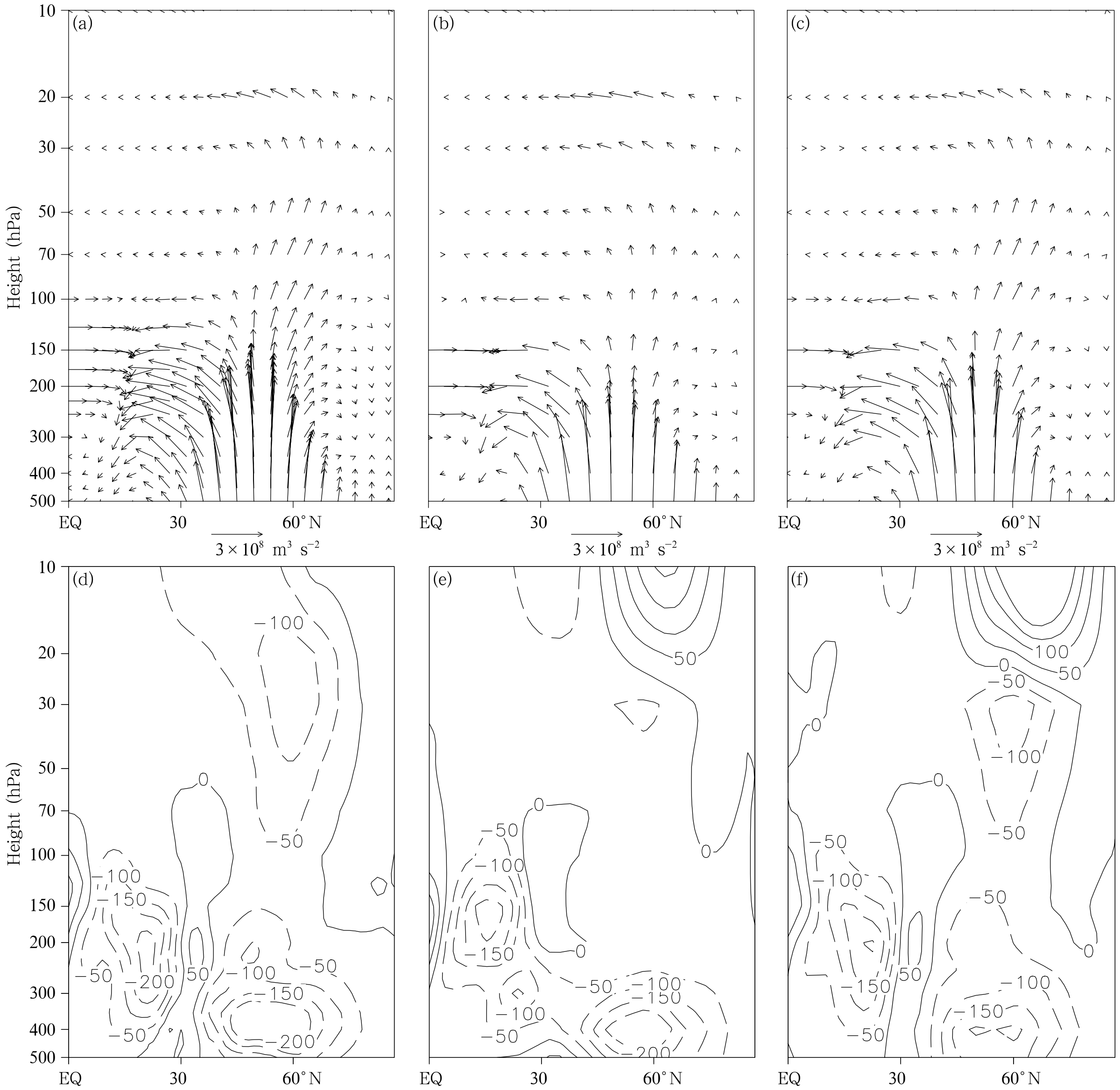

Fig. 3. Climatological mean (a, b, c) Eliassen-Palm (E-P) flux (m^3 s^{-2}) and (d, e, f) E-P flux divergence (m^2 s^{-2}) during January from the (a, d) ERA-Interim reanalysis, (b, e) NCEP/NCAR reanalysis, and (c, f) BCC_AGCM2.1. (Lu et al., 2014).

divergence in the planetary wave source region in the midlatitude troposphere (30°–60°N). The energy from perturbations largely resides in this region, propagating upward after convergence. Another area of strong E-P flux divergence is apparent over the subtropical region from the upper troposphere into the lower stratosphere. This region may be related to adjustments in the subtropical jet stream. The jet stream is located slightly higher in the model results than in the reanalysis, but its intensity and range are similar. Overall, BCC_AGCM2.1 simulates a dominant equatorward propagation of planetary waves, which is consistent with the reanalysis. Nevertheless, large errors remain between 100 and 20 hPa in the stratosphere over mid and high latitudes (particularly near 60°N). The ERA-Interim reanalysis indicates strong E-P flux divergence in this region. The E-P flux divergence simulated in this region by BCC_AGCM2.1 is relatively weak, leading to stronger circumpolar westerlies that prevent perturbations from entering the polar region and interacting with the stratospheric polar vortex.

Both BCC_AGCM2.1 and BCC_AGCM2.2 have been used to calculate 6–15-day extended forecasts of precipitation and other weather processes. Jie et al. (2013) reported improvements in 6–15-day forecasts of summer precipitation using a time-lagged ensemble approach with daily rainfall thresholds set to 1 and 5 mm day^{-1}, respectively. These improvements were particularly pronounced over the relatively wet areas in central and southern China, northeastern China, and the southeastern boundary of the Tibetan Plateau.

2.2 Land surface model

Land surface models describe exchanges of mass and energy in soils and at the land-atmosphere interface. These models are important components of climate system models. Chinese scientists have made substantial contributions to the development of land surface models. Ji (1995) developed the Atmosphere-Vegetation Interaction Model (AVIM), which accounts for biochemical processes like photosynthesis and vegetation respiration while also considering biophysical processes such as the exchange of heat and moisture among vegetation, soil, and atmosphere. The updated version AVIM2 (Ji et al., 2008) includes three modules. A land-surface physical process module describes radiation transfer through the vegetation canopy to the soil surface, as well as the exchange of moisture and heat among vegetation, air, and soil. The second module simulates eco-physiological processes during vegetation growth (e.g., photosynthesis, respiration, allocation of photosynthetic assimilated carbon, phenology, etc.). The third module provides a treatment of soil carbon decomposition.

The land surface model BCC_AVIM1.0 was developed as a component of BCC_CSM1.1 using the NCAR CLM3 and AVIM2 as a basis. BCC_AVIM1.0 includes a soil moisture and heat transfer module similar to that in CLM3, with underlying surfaces separated into four categories: soil, wetland, lake, and glacier. Soil is vertically discretized into 10 layers. Vegetation consists of one layer, with snow cover partitioned into as many as five layers depending on snow depth. Land vegetation is divided into 15 plant functional types (PFTs), with each model grid box containing up to 4 PFTs (Oleson et al., 2004). BCC_AVIM1.0 also includes a module that incorporates the parameterizations of vegetation dynamics and soil carbon decomposition from AVIM2 (Ji, 1995; Ji et al., 2008). This module describes the terrestrial carbon cycle, including CO_2 sequestration through photosynthesis, vegetation growth, and withering, and CO_2 release back into the atmosphere through soil respiration. The snow cover scheme takes into account multiple factors (e.g., snow depth, surface roughness, and sub-grid topography) for snow cover fraction (SCF). SCF is generally underestimated in CLM3 (Li et al., 2009), so this scheme has been modified to improve the simulation of SCF in regions with complex topography (such as the Tibetan Plateau and the Mongolian Plateau). BCC_AVIM1.0 serves as the land surface component in both BCC_CSM1.1 and BCC_CSM1.1(m), and is used for CMIP5 experiments. Wu et al. (2013) demonstrated the capacity of BCC_AVIM1.0 for simulating the land carbon cycle and terrestrial eco-systems during the 20th century.

The second generation of this model (BCC_AVIM2.0) is currently under development. Revisions will include changing the empirical plantleaf unfolding and withering dates prescribed in BCC_AVIM1.0 to a dynamic determination of leaf unfolding, growth, and withering dates according to the budget of photosynthetic assimilated carbon. This change will be similar to the phenology scheme used in CTEM (Arora, 2005). The method for identifying the threshold soil temperatures for freezing and thawing will also be modified (Xia et al., 2011), and a four-stream radiative transfer parameterization for the vegetation canopy will be incorporated (Zhou et al., 2010). These changes are expected to improve several aspects of the simulation, most notably the surface energy balance.

2.3 Global ocean general circulation model

The MOM4_L40 is a global Ocean General Circulation Model (OGCM) and a very important component of the climate system model BCC_CSM. This model has been developed by modifying the MOM4 model developed by the Geophysical Fluid Dynamics Laboratory (GFDL). The model is run on a global three-pole grid, in which the North Pole is imposed on both North America and the Eurasian continent. Its horizontal resolution is $1^{\circ}\times1^{\circ}$ poleward of 30°N and 30°S, incrementally descending to 1/3° latitude within 30°N and 30°S. The model has 40 vertical layers. The top 200 meters are divided into 20 layers of equal thickness (10 m). The physical process parameterization schemes (Griffies et al., 2005) include Swedy's tracer-based third order advection, isopycnic surface mixed tracer diffusion, Laplace horizontal friction, KPP vertical mixing, complete convective adjustment, and sea floor boundary/steep topography overflow processing that allows unstable gravity-driven fluid elements to flow down slope in the upstream advection scheme. The effects of spatial heterogeneities in chlorophyll are taken into account when calculating the penetration of short-wave solar irradiance. The ocean carbon cycle module from MOM4 FMS has been incorporated into MOM4_L40 to simulate the ocean carbon cycle. This module is based on the Ocean Carbon Model Intercomparison Project phase 2 (OCMIP2), and has a relatively well-integrated ocean carbon cycle.

MOM4_L40 is currently available in two versions (MOM4_L40v1 and MOM4_L40v2), which have different land and submarine topographies. MOM4_L40v1 is the ocean component of BCC_CSM1.1, while MOM4_L40v2 is the ocean component of BCC_CSM1.1(m). The treatment of inland seas in MOM4_L40v1 may cause unreasonable mass accumulation in those regions of the ocean. The land-sea masks in MOM_L40v2 have been adjusted to isolate inland seas. The results of the IPCC AR5 historical experiment indicate that both MOM4_L40v1 and MOM4_L40v2 can simulate the basic characteristics of the global oceans and ocean carbon budget reasonably well. Both models are also capable of reproducing major large-scale variability in the oceans. The next version (under development) will incorporate the wave-induced mixing scheme developed by the Institute of Oceanography, Chinese Academy of Sciences in Qingdao to better account for the roles of ocean waves (Qiao et al., 2004; Song et al., 2007).

2.4 Dynamic and thermodynamic sea ice model

The sea ice model is an important component of the climate system model. This model component has a major impact on global climate change through non-linear interactions with the atmosphere and ocean. The sea ice model used in both BCC_CSM1.1 and BCC_CSM1.1(m) is the Sea Ice Simulator (SIS), a dynamic/thermodynamic sea ice model developed at GFDL (Winton, 2000). The horizontal resolution and sea-land distribution of the model are identical to those used in the ocean model (MOM_L40v1 or MOM4_L40v2, respectively). This model describes sea ice thermodynamic processes according to the model developed by Semtner (1976). The model has three layers in the vertical direction (i.e., a snow cover layer and two sea ice layers of equal thickness), and divides sea ice into five categories based on thickness. It is assumed that snow cover has no heat capacity, but all sea ice layers have sensible heat capacity. The effects of high-salinity bubbles on heat capacity are considered in the upper layer. The model uses viscoelastic plasticity to calculate the internal stress of the sea ice, and adopts an upwind scheme for calculations of conserved quantities (e.g., sea ice density, total ice, and the heat capacity of sea ice) and other advective processes. The results of the CMIP5 multi-model intercomparison indicate that BCC_CSM1.1 gives a relatively good simulation of sea ice in the Southern Hemisphere, but slightly overestimates sea ice during the winter half year in the Northern Hemisphere and underestimates sea ice during the summer half year. Overall, the model is capable of simulating decadal changes in sea ice over the 20th century.

2.5 Climate system models

2.5.1 BCC_CSM1.0

BCC_CSM1.0 was developed using the NCAR Community Climate System Model version 3 (CCSM3) as a basis. This model has coupled BCC_AGCM2.0 with the land surface process model

CLM3, the global ocean circulation model POP, and the global dynamic/thermodynamic sea ice model CISM. This model version was fully developed by the end of 2008. BCC_CSM1.0 has been shown to have a stable performance in a number of experiments similar to the multi-model intercomparions performed during the 20th century (such as CMIP3 for IPCC AR4). The simulated increase of global surface air temperature from the late 19th century to the late 20th century is consistent with HadCRUT3 observations (Brohan et al., 2006) when the model is forced by observed changes in GHGs, solar activity, and aerosols. This consistency indicates that BCC_CSM1.0 is in the same class as the coupled models that participated in the intercomparisons for IPCC AR4 (Editorial Committee of National Assessment Report of Climate Change, 2011).

BCC_CSM1.0 can simulate the basic climate state, seasonal changes, interseasonal oscillations, and interannual variations of global precipitation reasonably well (Zhang Li et al., 2012; Dong et al., 2013). It can also reproduce the climatology of summer precipitation over East Asia (Fig. 4). Simulations of interannual changes in mean summer precipitation over East Asia or China during 1979–2000 by BCC_CSM1.0 have relatively high correlations with the Xie-Arkin precipitation dataset. The root-mean-square errors are also relatively small. Zhang et al. (2011) demonstrated that the model is able to capture precipitation and temperature extremes in East Asia.

2.5.2 BCC_CSM1.1 and BCC_CSM1.1(m)

BCC_CSM1.1 is also based on the CCSM3 developed at NCAR. This model fully couples the atmospheric-model BCC_AGCM2.1, the land surface

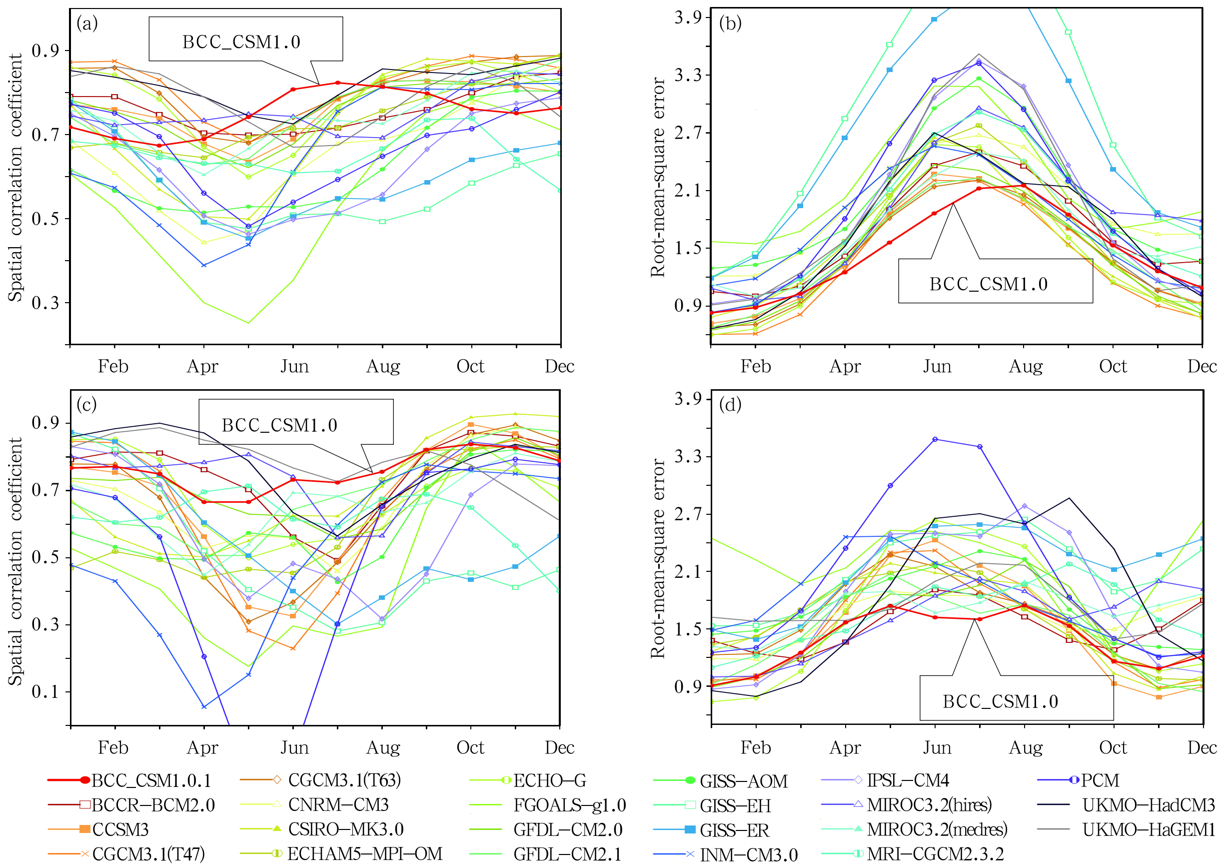

Fig. 4. (a, c) Spatial correlation coefficients and (b, d) root-mean-square errors for mean monthly precipitation over 1979–1999 from models participating in the IPCC AR4 intercomparison, relative to the Xie-Arkin precipitation data for the same period. (a, b) China and (c, d) all of East Asia.

model BCC_AVIM1.0, the global ocean circulation model MOM4_L40v1, and the global dynamic/thermodynamic sea ice model SIS using a flux coupler. Detailed descriptions of these models are provided by Wu et al. (2013). This model can simulate changes in atmospheric CO_2 concentration from anthropogenic emissions as well as the impacts of these changes on global climate. BCC_CSM1.1 is one of the several earth system models participating in the multi-model intercomparisons for IPCC AR5, and performs well in simulating the global carbon cycle (Wu et al., 2013) and its feedback to climate (Arora et al., 2013).

BCC_CSM1.1(m) is an upgraded version of BCC_CSM1.1. BCC_CSM1.1(m) uses a horizontal resolution of T106 in the atmosphere and land component models and the same ocean-sea ice resolutions as BCC_CSM1.1. The atmospheric component model is BCC_AGCM2.2, and the ocean component model is MOM4_L40v2.

Both BCC_CSM1.1 and BCC_CSM1.1(m) have participated in most of the CMIP5 experiments (Xin et al., 2012) and have provided a large amount of simulation output for use in climate studies. More than 140 peer reviewed journal papers (as of Nov. 8, 2013) have analyzed output from the BCC_CSM1.1 model (http://cmip.llnl.gov/cmip5/publications/model). The performance of both models is comparable to that of other CMIP5 models with similar resolutions with respect to cloud microphysics and carbon-climate feedbacks (Jiang et al., 2012; Arora et al., 2013; Su et al., 2013). BCC_CSM1.1 provides a reasonable simulation of the upper tropospheric jet streams and related transient vortex activity over East Asia (Xiao and Zhang, 2012). The decadal prediction experiments performed under CMIP5 show that the model is capable of accurately predicting global mean surface air temperatures on decadal scales. Decadal climate predictions using BCC_CSM1.1 have the highest skill in mid and higher latitudes over the Indian Ocean in the Southern Hemisphere, the tropical West Pacific, and the tropical Atlantic (Gao et al., 2012). The following section evaluates simulations of the 20th century climate, the climate of the last millennium, and climate change over the next century using BCC_CSM1.1 and BCC_CSM1.1(m).

3. Climate simulations and projections using the BCC_CSM

3.1 Simulations of the 20th century climate

3.1.1 Surface air temperature

Evaluation of the mean state of present-day climate in coupled models is important evidence of their simulation capabilities. Given external forcing by observed GHGs, natural and anthropogenic aerosols, volcanic eruptions, total column ozone, and solar activity, both BCC_CSM1.1 and BCC_CSM1.1(m) effectively capture the global distribution of annual mean surface air temperature averaged over 1971–2000 (Fig. 5). Significant biases relative to the ERA40 reanalysis (Uppala et al., 2005) are concentrated in the polar areas and regions of complex topography (such as Antarctica, Greenland, the Tibetan Plateau, the eastern coast of Africa, and the Andes along the west coast of South America). The temperature simulated by the model near Greenland is over 10℃ colder than the reanalysis estimate, while temperatures over parts of Antarctica and the Tibetan Plateau are more than 6℃ warmer than the corresponding reanalysis estimates. Model biases over Greenland and in the Antarctic region may be associated with problems in the simulation of sea ice, while the large temperature bias over the Tibetan Plateau may be due to differences between the topography in the model and that of the actual terrain. Outside of these regions, absolute temperature biases are within ±2℃ over most other regions. These biases are similar to those of models participating in the CMIP3 multi-model intercomparison summarized in AR4 (Trenberth et al., 2007). The simulation of surface air temperature by BCC_CSM1.1(m) represents a slight improvement over that by BCC_CSM1.1. The RMSE has reduced from 2.37 K in BCC_CSM1.1 to 2.07 K in BCC_CSM1.1(m). Biases in surface air temperature also decrease over some regions, most notably Greenland and East Asia.

3.1.2 Precipitation

Precipitation is also a very important variable for evaluating model performance. Most of the 20 climate

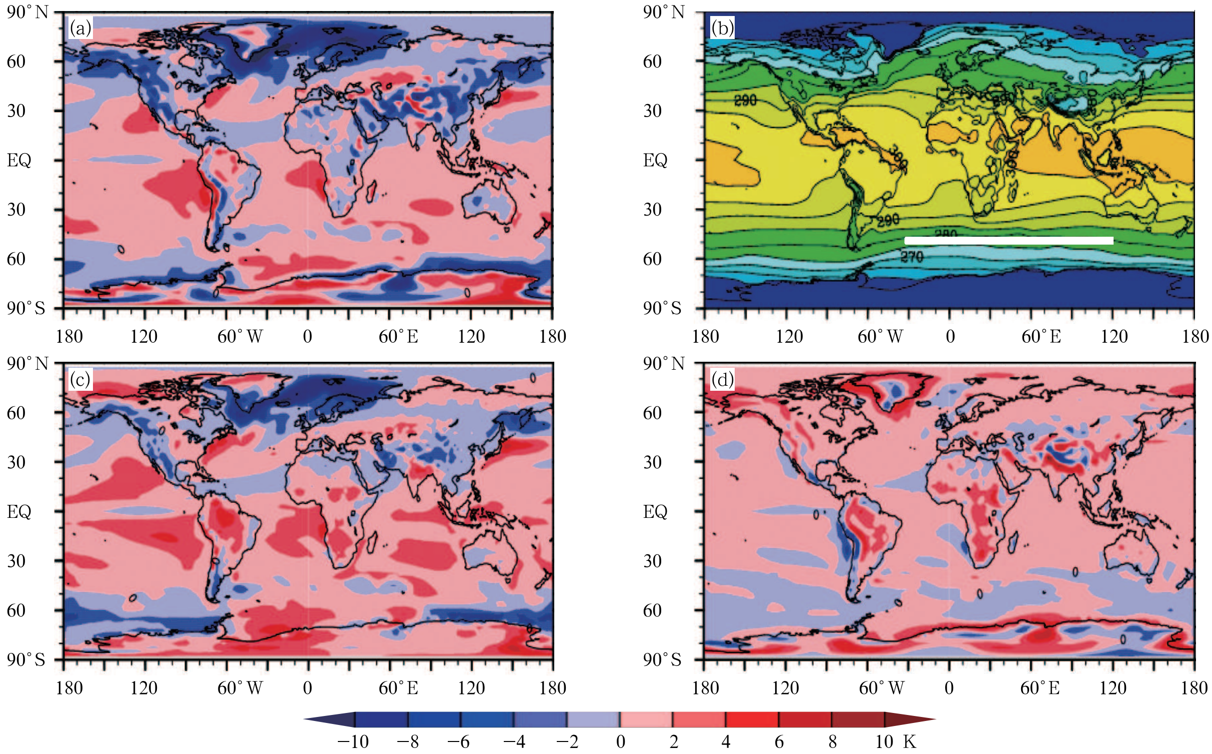

Fig. 5. Annual-mean surface air temperature (K) averaged over 1971–2000 from (b) ERA40 reanalysis, biases relative to ERA40 for (a) BCC_CSM1.1 and (c) BCC_CSM1.1(m), and (d) difference (°C) between the two versions of the BCC_CSM

system models evaluated and analyzed for the IPCC AR4 are able to capture the large-scale zonal mean distribution of precipitation. Both BCC_CSM1.1 and BCC_CSM1.1(m) can simulate the basic geographic distribution of precipitation during the solstice seasons (Fig. 6). The correlation coefficient between simulations and observations is greater than 0.8 (Zhang et al., 2013), suggesting that these two models capture the basic characteristics of the atmospheric circulation reasonably well. Both BCC_CSM1.1 and BCC_CSM1.1(m) reproduce rainy zones in the ITCZ region over the equatorial Pacific, the South Pacific Convergence Zone (SPCZ), the Northwest Pacific region, the equatorial South Indian Ocean, and tropical Africa.

Some significant asymmetries and biases still exist in these simulations of precipitation. For example, a double ITCZ appears in the tropical Pacific region during boreal winter (DJF; see Fig. 6) and spring (MAM; figure omitted). This feature is particularly pronounced in BCC_CSM1.1(m). Biases in annual mean precipitation (figure omitted) manifest mainly in the high precipitation area of the equatorial Pacific ITCZ, which is slightly weak and shifted northward relative to observations. Rainfall over the central-eastern South Pacific is overestimated (leading to a positive-negative-positive chain of biases from north to south over this region), while precipitation over the Indian Ocean is underestimated. The high precipitation area over North Pacific is located too far to the north, and the intensity of precipitation in this region is slightly exaggerated. Precipitation over the equatorial region in northwestern South America is overestimated, while rainfall over the equatorial area along the northeastern Atlantic Ocean is underestimated. Rainfall amounts over equatorial Africa and the Eurasian continent are slightly too high, especially on and around the Tibetan Plateau.

The distribution of precipitation in BCC_CSM1.1(m) is improved relative to that in BCC_CSM1.1 in many regions, but not all. The negative

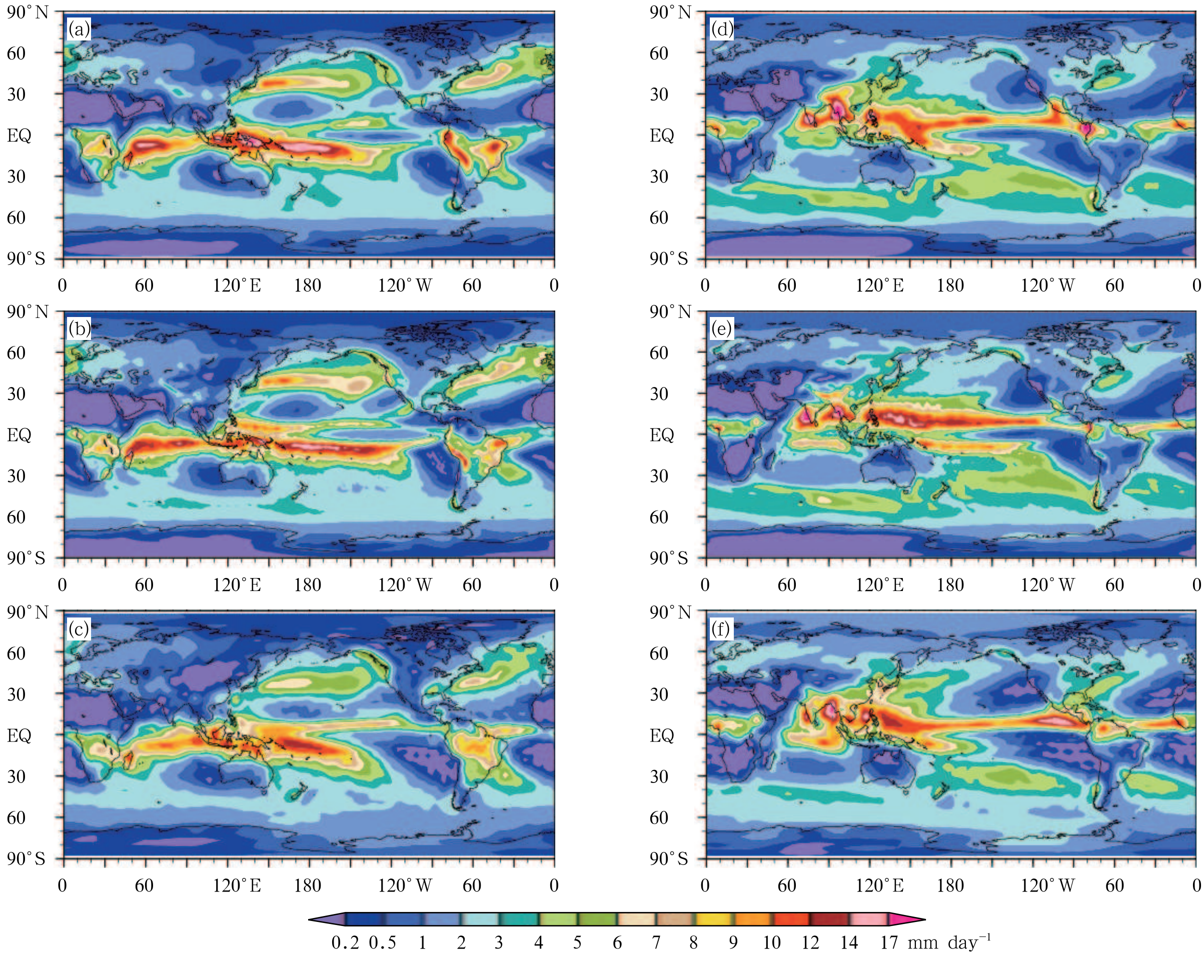

Fig. 6. Mean precipitation for (a, b, c) DJF and (d, e, f) JJA from (a, d) BCC_CSM1.1, (b, e) BCC_CSM1.1(m), and (c, f) the Xie-Arkin observational data.

precipitation bias over the South Indian Ocean is reduced, the positive precipitation biases over northwestern South America and the Tibetan Plateau are reduced, and the negative precipitation bias over the equatorial Pacific changes to positive. However, the negative precipitation bias over East Asia is increased, the double ITCZ is even more prevalent, precipitation in the SPCZ extends too far toward the east and not far enough toward the south, and the positive precipitation bias over the central South Pacific is increased. The overall spatial distribution of climatological mean precipitation is more realistic in BCC_CSM1.1(m) than in BCC_CSM1.1 (Su et al., 2013).

Both BCC_CSM1.1 and BCC_CSM1.1(m) can reconstruct the basic distributions of the annual tropical precipitation mode, including the equatorial antisymmetric structure of precipitation and the atmospheric circulation in the monsoon mode and the north-south anti-phase distribution of the equinoctial asymmetric mode over the tropical Pacific and Atlantic. These aspects of the simulations have been described in detail by Zhang et al. (2013).

Figure 7 shows the annual cycle of mean precipitation by latitude over East Asia. These annual cycles have been averaged over the longitudinal belts 110°–120°E and 130°–140°E to represent the seasonal cycles of rainfall over land and sea, respectively. Both BCC_CSM1.1 and BCC_CSM1.1(m) capture the seasonal movement of the precipitation band over East Asia reasonably well, although they have difficulties reproducing the exact timing and amount of precipi-

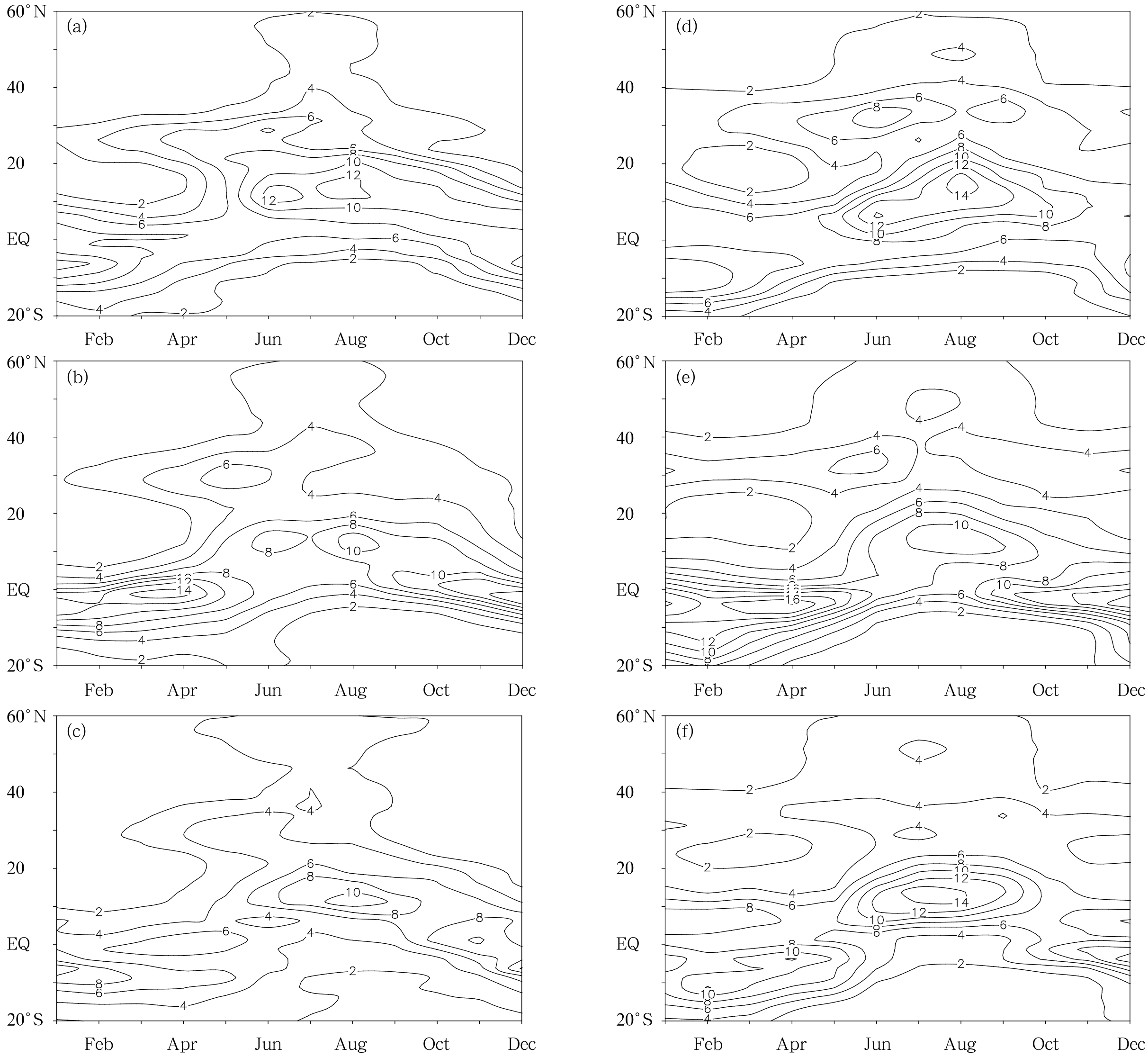

Fig. 7. Seasonal precipitation evolution over East Asia from (a, d) the CMAP observational data, (b, e) BCC_CSM1.1, and (c, f) BCC_CSM1.1(m) averaged over the longitude belts (a, b, c) 110°–120°E and (d, e, f) 130°–140°E.

tation. The northward movement and southward retreat of mean precipitation averaged from 110°–120°E (Figs. 7a–c) indicate that the simulated precipitation center from 5° to 10°S in winter is located slightly too far to the north, and that the intensity and duration of this precipitation center are overestimated. The timing at which the 4 mm day^{-1} contour line first enters the area south of the Yangtze River is delayed by 1 month in the simulations (early March) relative to the observations (early February). The position of this contour also seems to be shifted too far to the north. These biases are even more pronounced in BCC_CSM1.1(m). BCC_CSM1.1 underestimates precipitation during the rainy season over the area south of 30°N (especially in South China), but it overestimates the precipitation over the region north of 30°N. Precipitation in the 30°–40°N latitude band is too large by approximately 2 mm day^{-1} relative to the observations, and the simulated rainband is shifted too far to the north. The biases in precipitation intensity in this region are reduced in BCC_CSM1.1(m) relative to BCC_CSM1.1, although BCC_CSM1.1(m) still underestimates rainfall in the region south of 35°N and slightly overestimates precipitation in the area north of 35°N.

The observed seasonal movement of precipitation averaged over the 130°–140°E longitudinal band indicates that the rainband is quasi-stationary near 10°S from December to February, while precipitation is weak from 30°–40°N (Fig. 7d). Both models simulate this basic feature, although the precipitation center in the Southern Hemisphere is shifted slightly too far north in BCC_CSM1.1, with a longer duration and higher intensity (by 4 mm day^{-1}) than observed. The precipitation intensity in the area of weak precipitation in the north is also overestimated, and the location of this area is again shifted slightly too far to the north. The BCC_CSM1.1(m) simulation of precipitation intensity in the region south of the equator is closer to the observed precipitation intensity than the BCC_CSM1.1 simulation. The observations indicate that the center of maximum precipitation reaches 5°N in early May. This transition is delayed until late May or early June in the BCC_CSM1.1 simulation, and both the duration and intensity of this precipitation center are underestimated. The simulated transition in BCC_CSM1.1(m) also lags slightly behind the observations, but the rainband is pushed slightly too far to the north with an intensity very close to the observed intensity. The BCC_CSM1.1(m) simulation is closer to the observations with respect to the timing, location, and intensity of the rainband. Both models underestimate the observed intensity of the precipitation center near 30°N, and the simulated 2 mm day^{-1} rainbands do not move far enough north.

3.2 Simulations of climate during the last millennium

Although human influences on the climate system have increased substantially since the industrial revolution, it is instructive to view the warming of the 20th century (20CW) from the perspective of a longer timescale. In particular, this perspective enhances understanding of the mechanisms and evolution of climate change. The Medieval Climate Anomaly (MCA) and the Little Ice Age (LIA) are two typical periods of global-scale warming and cooling, respectively, within the last millennium. The warming during the MCA may have approached or even exceeded the warming in the 20th century in some areas (Moberg et al., 2005; Guiot et al., 2010). Comparisons of climatic characteristics during the MCA, LIA, and 20CW periods can reveal the roles and contributions of natural variability and human activity to climate change. This technique is especially useful for exploring the mechanisms behind climate evolution during different periods, such as the natural medieval warming and the recent centennial warming.

"Climate modeling for the past millennium (past1000)" is one of the core experiments in CMIP5. This experiment is helpful for evaluating model stability and transient response under different external forcings. These external forcings include annual variations in the solar constant, volcanic activity, and GHG concentrations from 850 to 2000 AD. Figure 8 shows the evolution of the Northern Hemisphere mean surface temperature from BCC_CSM1.1 and 11 proxy reconstructions of surface temperature over the same domain. The uncertainties and deviations in the reconstructed time series of surface temperature are large due to the limited quantity and quality of the underlying proxy data. The model simulations of surface temperature during the MCA are underestimated relative to the reconstructions. Aside from the uncertainties in the surface temperature reconstructions, this bias may reflect uncertainties in the external forcings and the model initial state. The agreement between the reconstructed data and the simulations is greater during the LIA period. The model reproduces three cold periods during the LIA: Spörer (1450–1540), Maunder (1645–1715), and Dalton (1790–1820). The climate evolution and sensitivity simulated by BCC_CSM1.1 are reasonable relative to the simulations submitted from four other participating models (CCSM_4, CSIRO-Mk3L, GISS-E2-R, and MPI-ESM-P). Simulated surface temperatures are warmer during the MCA period than during the LIA period by 0.05–0.21℃. The value simulated by BCC_CSM1.1 is approximately 0.11℃, well within this range. Further analyses of these simulations are under way.

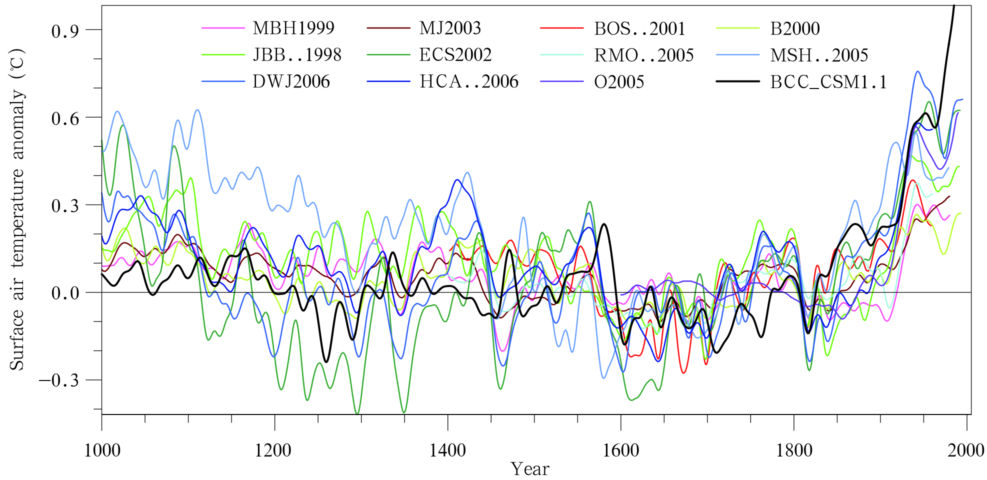

Fig. 8. Anomalies in surface temperature (relative to the 1500–1899 mean) over the Northern Hemisphere as simulated by BCC_CSM1.1 (black line). The colored lines represent 11 reconstructions of mean surface temperature (cf. Fig. 6. 10b from Jansen et al., 2007). All curves are smoothed using a 30-yr low-pass filter.

3.3 Simulations of the last 100 years and projections of future climate change

The ability of a climate system model to reproduce the 20th century climate is an important indicator of its performance and a useful criterion for judging the reliability of its future climate change projections. Xin et al. (2013b) have evaluated changes in the global mean air temperature from 1861 to 2005 simulated by the two climate system models developed at the NCC, China and 18 other CMIP5 models. All of these models reproduce the global warming trend over the 20th century, including the especially significant warming over the last 50 years of the century (Fig. 9a). The simulations by the two NCC models are largely consistent with the multi-model ensemble mean; however, they slightly overestimate the observed warming trend in the 20th century. The mean temperature simulated for the early 21st century (2000–2005) has increased by 0.45℃ in BCC_CSM1.1 and 0.62℃ in BCC_CSM1.1(m) relative to the mean value for 1971–2000. Both of these simulated increases are larger than the observed increase (0.33℃). The magnitude of the warming simulated by BCC_CSM1.1 is closer to the multi-model mean (0.48℃) than the magnitude of the warming simulated by BCC_CSM1.1(m). This result stems from the relative proximity of the climate sensitivity in BCC_CSM1.1 to the multi-model mean climate sensitivity. The climate sensitivity is higher in BCC_CSM1.1 (Zhang Li et al., 2012). Correlations between simulated and observed values can reflect a model's ability to capture interannual variations in temperature. Over the period 1861–2005, the correlation coefficient between the BCC_CSM1.1 simulation and observations is 0.88, while that between the BCC_CSM1.1(m) simulation and observations is 0.83. The correlation coefficient between the multi-model ensemble mean and observations is 0.88. The relatively large value of this correlation coefficient suggests that the multi-model ensemble mean value can better represent the level of model simulations than can a single model (Zhou and Yu, 2006; Sun and Ding, 2008; Annan and Hargreaves, 2011). BCC_CSM1.1 is therefore regarded as being able to capture interannual variations in global mean temperature. Almost all of the coupled models have difficulties reproducing the relative warmth of the early 20th century (approximately 1920–1940). These difficulties may be related to errors in assumed solar radiation, volcanic activity or other natural external forcing factors, or in the representation of the synergistic internal variability of the climate system. The relative coolness of the 1960–1970 period may be linked to the strong eruption of the Agung volcano in 1963. There have been several strong volcanic eruptions over the past 150 years, such as Krakatoa in 1883, Pelee in 1902, and Pinatubo in 1991. The cooling effect of volcanic aerosols injected into the atmosphere by these eruptions may have caused brief periods of relatively low temperatures in the time series of global mean temperature.

Figure 9b shows surface air temperature anomalies averaged over China as simulated by 20 CMIP5 models. Each value is the sum of averages in three areas within the China domain (28°–50°N, 80°–97.5°E; 22.5°–43°N, 97.5°–122.5°E; and 43°–54°N, 117.5°–130°E). The range of mean surface air temperature anomalies over China is even larger than the range of global mean temperature anomalies. The simulations by BCC_CSM1.1 and BCC_CSM1.1(m) are similar to the multi-model ensemble mean, suggesting that both models can simulate warming over China during the 20th century. Both models simulate temperature increases of 0.48℃ in the early 21st century (2000–2005) relative to the 1971–2000 climatological mean. These increases are lower than both the multi-model ensemble mean increase (0.63℃) and the observed increase (0.69℃). The correlation coefficient between BCC_CSM1.1 and observations during 1906–2005 is 0.50, while that between BCC_CSM1.1(m) and observations is 0.55. This result indicates that these two models are able to simulate interannual changes in surface air temperature over China during the past century reasonably well. The higher-resolution BCC_CSM1.1(m) performs slightly better than BCC_CSM1.1. The best simulation of interannual temperature changes over China is by the high-resolution Japanese MIROC4h, with a correlation coefficient of 0.6. Many studies have explored the spatial distribution of recent climate change in China. For example, the BCC_CSM1.1 model is able to capture changes in springtime rainfall over eastern China (Xin et al., 2013a).

New Representative Concentration Pathway (RCP) emission scenarios are used in CMIP5 projections of climate change in the 21st century. Those scenarios are named according to the intensity of the radiative forcing in 2100: RCP8.5, RCP6, RCP4.5, and RCP2.6. Figure 10 shows projections of mean surface air temperature over China from 13 CMIP5 models (including BCC_CSM1.1 and BCC_CSM1.1(m)) under the RCP2.6, RCP4.5, and RCP8.5 scenarios. Almost all the models project continued increases in temperature over China under all three scenarios. Under RCP2.6, the models project that mean temperature over China would peak around 2050, remain virtually stable from 2050 to 2070, and then decrease from 2070 to the end of the 21st century. Projected changes in global mean temperatures are similar (Xin et al., 2012). Under RCP4.5, the temperature over China would increase through 2100, although the rate of this increase would slow toward the end of the 21st century. Under RCP8.5, all models project continued increases in mean temperature over China through the end of the 21st century. BCC_CSM1.1 and BCC_CSM1.1(m) are largely consistent with the multi-model ensemble mean under each of the three scenarios. This multi-model mean projects that mean temperature over China would increase by 1.4℃ under RCP2.6, 2.5℃ under RCP4.5, and 5.7℃ under RCP8.5. Xin et al. (2013c) also analyzed the changes in precipitation over East Asia projected to occur by the end of the 21st century according to BCC_CSM1.1 under all four RCP scenarios. They found that the simulated East Asian monsoon strengthens under the medium and high emissions scenarios, while the summer mean precipitation over the Yangtze River basin decreases and the precipitation over North China increases (figure omitted).

4. Summary

This paper provides an overview of progress in the development of the global atmospheric general circulation, land surface, ocean general circulation, and sea ice component models of the fully coupled climate system models constructed by the National Climate Center (NCC). The main features of the two climate system models and their component models are described. Their performance is then evaluated by applying several basic metrics to the large amount of data generated for CMIP5. Particular attention is paid to simulations of precipitation and temperature

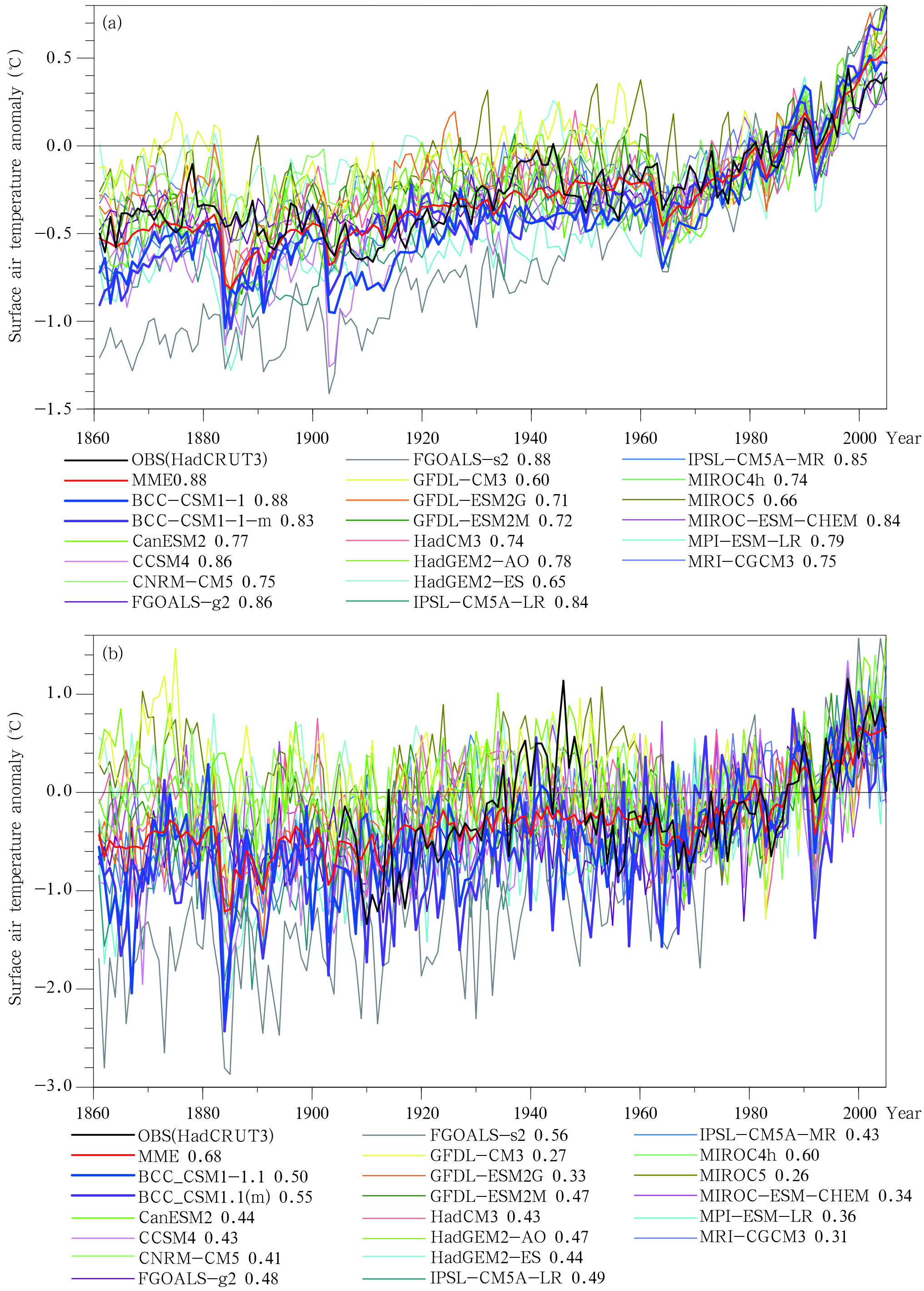

Fig. 9. Anomalies in annual mean surface air temperature (℃) between 1861 and 2005 relative to the 1971–2000 mean over (a) the whole globe and (b) China. The results are shown for BCC_CSM1.1, BCC_CSM1.1(m), and 18 other CMIP5 models. The solid black curve indicates the observed time series, the solid red curve indicates the ensemble average from 20 members, and the thin curves indicate simulations by individual models. The numbers listed in the legend indicate correlation coefficients between the listed model simulation and observations (global observations from HadCRUT3, Brohan et al., 2006; China observations from Tang and Ren, 2005; redrawn by Xin et al., 2013c).

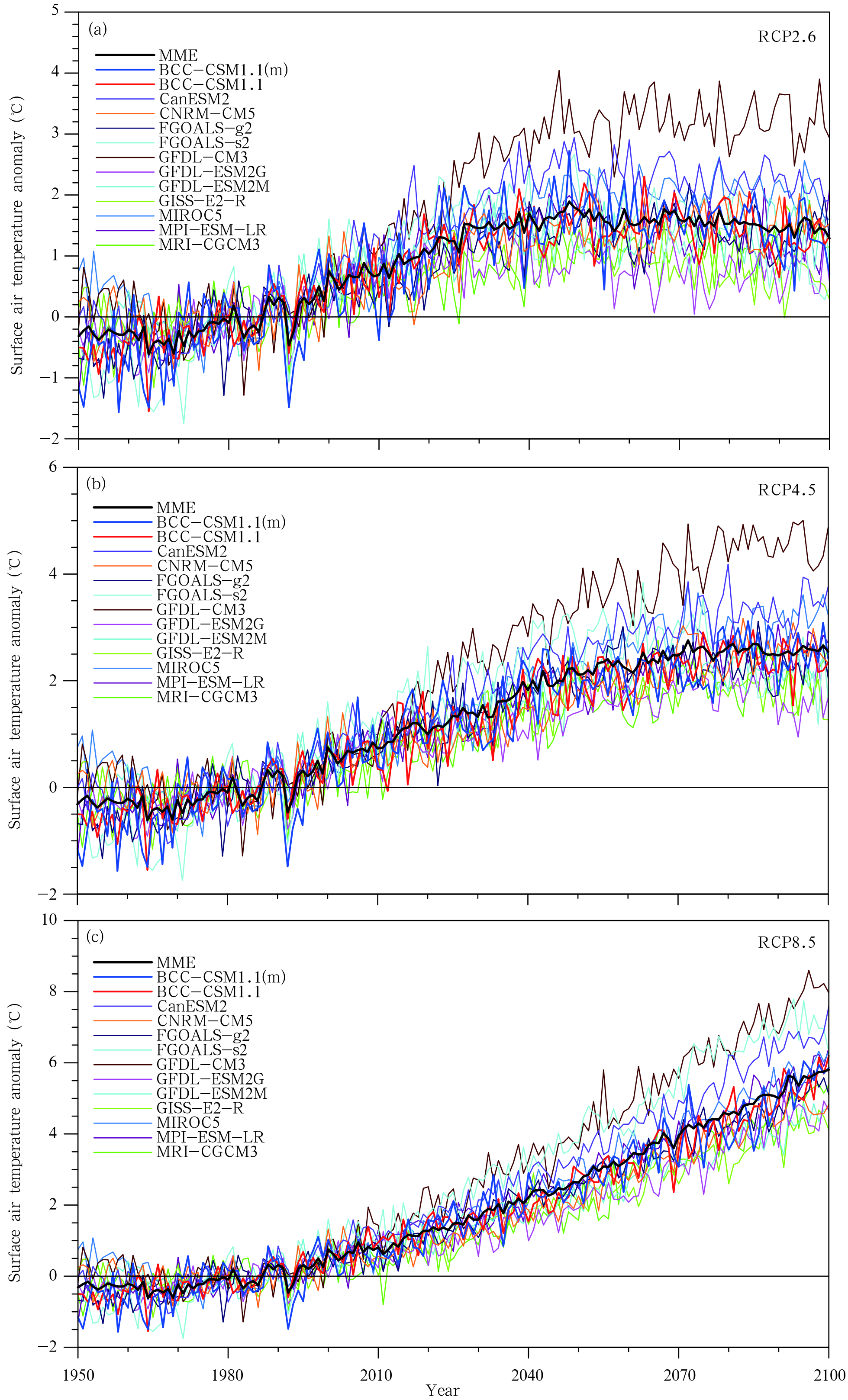

Fig. 10. Anomalies of annual-mean surface air temperature (℃) relative to the 1971–2000 mean under three RCP emission scenarios for BCC_CSM1.1, BCC_CSM1.1(m), and other CMIP5 models. The solid black line represents the multi-model ensemble mean. The thin curves indicate simulations from individual models.

in present-day climate and simulations of temperature changes over the past millennium. Differences in simulations of climate change over the past 100 years and projections of climate change over the next 100 years between BCC_CSM1.1, BCC_CSM1.1(m), and other CMIP5 models have also been assessed. The major conclusions can be summarized as follows.

(1) The second-generation AGCMs developed at NCC (i.e., BCC_AGCM2.0, BCC_AGCM2.1, and BCC_AGCM2.2) include substantial improvements to the dynamic framework and physical processes. These models have demonstrated relatively good performance in simulations of current climate, including surface air temperature, precipitation, stratospheric temperature, and the atmospheric circulation. Model representations of seasonal changes, extreme temperatures, heavy precipitation, and tropical intraseasonal oscillations are also relatively realistic. Increasing the horizontal resolution of BCC_AGCM has improved simulations of the regional distribution of precipitation to some extent.

(2) The land surface model BCC_AVIM is capable of simulating vegetation dynamics and the land surface carbon cycle. BCC_AVIM is a component of both BCC_CSM1.1 and BCC_CSM1.1(m).

(3) BCC_CSM_1.0, BCC_CSM1.1, and BCC_CSM1.1(m) have shown a good ability to simulate the mean climate state, long-term trends, and interannual climate changes when forced by observed GHGs, aerosols, volcanic eruptions, total column ozone, and solar variability. Simulated values of global mean temperature changes are close to the ensemble means of models participating in the CMIP3 and CMIP5 intercomparisons. The largest biases are found in polar areas, the Tibetan Plateau region, and other areas with complex topography. The simulation of the surface air temperature climatology by the higher-resolution BCC_CSM1.1(m) is more realistic than that by BCC_CSM1.1.

(4) Both BCC_CSM1.1 and BCC_CSM1.1(m) provide reasonable simulations of the spatial distributions of annual and seasonal mean precipitation. BCC_CSM1.1(m) is better in simulating regional precipitation, but both models still contain obvious deficiencies (such as a double ITCZ in the tropical Pacific, which is especially pronounced in BCC_CSM1.1(m)). Precipitation over East Asia is generally less intense than observed in both models.

(5) BCC_CSM1.1 can simulate global warming and cooling episodes during the past millennium, including the Medieval Climate Anomaly (MCA) and Little Ice Age (LIA).

(6) BCC_CSM1.1 and BCC_CSM1.1(m) can simulate global climate change on centennial scales. The overall performance of each model is comparable to that of other CMIP5 models with similar resolutions. Output from the two models is generally consistent with the CMIP5 multi-model ensemble mean, although both models slightly overestimate the observed warming trend during the 20th century. BCC_CSM1.1 projects that mean temperature over China would increase by 1.4℃ under RCP2.6, 2.5℃ under RCP4.5, and 5.7℃ under RCP8.5 by the end of the 21st century. These projections are consistent with the CMIP5 multi-model ensemble mean.

(7) BCC_CSM1.1 and BCC_CSM1.1(m) are earth system models that can be used to simulate interannual changes in the global concentration of atmospheric CO_2 under anthropogenic carbon emission scenarios. These models have a preliminary capacity for simulating the global carbon cycle.

Acknowledgments. The language editor for this manuscript is Dr. Jonathon S. Wright.

REFERENCES

Annan, J. D., and J. C. Hargreaves, 2011: Understanding the CMIP3 multimodel ensemble. *J. Climate*, **24**, 4529–4538.

Arora, V. K., and G. J. Boer, 2005: A parameterization of leaf phenology for the terrestrial ecosystem component of climate models. *Global Change Biol.*, **11**, 39–59, doi: 10.1111/j.1365-2486.2004.00890.x.

—, —, P. Friedlingstein, et al., 2013: Carbon-concentration and carbon-climate feedbacks in CMIP5 earth system models. *J. Climate*, **26**, 5289–5314, doi: 10.1175/JCLI-D-12-00494.1.

Brohan, P., J. J. Kennedy, I. Harris, et al., 2006: Uncertainty estimates in regional and global observed temperature changes: A new data set from 1850. *J. Geophys. Res.*, **111**, D12106, doi: 10.1029/2005JD006548.

Chen Haishan, Shi En, and Zhou Jing, 2011: Evaluation of recent 50 years extreme climate events over China simulated by Beijing Climate Center (BCC) climate model. *Trans. Atmos. Sci.*, **34**(5), 513–528. (in Chinese)

Chen Haoming, Yu Rucong, Li Jian, et al., 2012: The coherent interdecadal changes of East Asian climate in mid summer simulated by BCC_AGCM 2.0.1. *Climate Dyn.*, **39**, 155–163, doi: 10.1007/s00382-011-1154-6.

Collins, W. D., P. J. Rasch, B. A. Boville, et al., 2004: Description of the NCAR Community Atmosphere Model (CAM3.0). NCAR/TN-464+STR, 214 pp.

Ding Yinghui, Liu Yiming, Song Yongjia, et al., 2002: Research and experiments of the dynamical model system for short-term climate prediction. *Climatic Environ. Res.*, **7**(2), 236–246. (in Chinese)

——, Li Qingquan, Li Weijing, et al., 2004: Advance in seasonal dynamical prediction operation in China. *Acta Meteor. Sinica*, **62**(5), 598–612. (in Chinese)

——, Ren Guoyu, Shi Guangyu, et al., 2006: National assessment report of climate change. Part I: Climate change in China and its future trend. *Adv. Climate Change Res.*, **2**(1), 3–8. (in Chinese)

Dong Min, 2001: *Introduction to National Climate Center Atmospheric General Circulation Model–Basic Principles and Applications*. China Meteorological Press, Beijing, 152 pp. (in Chinese)

——, Wu Tongwen, Wang Zaizhi, et al., 2009: Simulations of the tropical intraseasonal oscillation by the atmospheric general circulation model of the Beijing Climate Center. *Acta Meteor. Sinica*, **67**(6), 912–922.

——, ——, ——, et al., 2012: A simulation study on the extreme temperature events of the 20th century by using the BCC_AGCM. *Acta Meteor. Sinica*, **26**(4), 489–506, doi: 10.1007/s13351-012-0408-5.

——, ——, ——, et al., 2013: Simulation of the precipitation and its variation during the 20th century using the BCC climate model (BCC_CSM_1.0). *J. Appl. Meteor. Sci.*, **24**, 1–11. (in Chinese)

Editorial Committee of National Assessment Report of Climate Change, 2011: *Second National Assessment Report of Climate Change*. Science Press, Beijing, 710 pp.

Gao Feng, Xin Xiaoge, and Wu Tongwen, 2012: A study of the prediction of regional and global temperature on decadal time scale with BCC_CSM1.1 model. *Chinese J. Atmos. Sci.*, **36**(6), 1165–1179, doi: 10.3878/j.issn.1006-9895.2012.11243. (in Chinese)

Gong, S. L., L. A. Barrie, and M. Lazare, 2002: Canadian Aerosol Module (CAM): A size-segregated simulation of atmospheric aerosol processes for climate and air quality models 2. Global sea-salt aerosol and its budgets. *J. Geophys. Res.*, **107**(D24), AAC 13-1-AAC 13-14, doi: 10.1029/2001JD002004.

——, ——, J. P. Blanchet, et al., 2003: Canadian aerosol module: A size-segregated simulation of atmospheric aerosol processes for climate and air quality models 1. Module development. *J. Geophys. Res.*, **108**, AAC 3-1-AAC 3-16, doi: 10.1029/2001JD002002.

Griffies, S. M., A. Gnanadesikan, K. W. Dixon, et al., 2005: Formulation of an ocean model for global climate simulations. *Ocean Sci.*, **1**, 45–79.

Guiot, J., C. Corona, ESCARSEL members, 2010: Growing season temperatures in Europe and climate forcings over the past 1400 years. *PLOS ONE*, **5**(4), e9972. doi: 10.1371/journal.pone.0009972.

Guo Zhun, Wu Chunqiang, Zhou Tianjun, et al., 2011: A comparison of cloud radiative forcings simulated by LASG/IAP and BCC atmospheric general circulation models. *Chinese J. Atmos. Sci.*, **35**(4), 739–752. (in Chinese)

Hack, J. J., 1994: Parameterization of moist convection in the National Center for Atmospheric Research Community Climate Model (CCM2). *J. Geophys. Res.*, **99**, 5551–5568.

Jansen, E., J. Overpeck, K. R. Briffa, et al., 2007: *Palaeoclimate. Climate Change 2007: The Physical Science Basis*. Solomon, S., D. Qin, M. Manning, et al., Eds., Cambridge University Press, Cambridge, United Kingdom and New York, NY, USA.

Ji Jinjun, 1995: A climate-vegetation interaction model: simulating physical and biological processes at the surface. *J. Biogeography*, **22**, 445–451.

——, Huang Mei, and Li Kerang, 2008: Prediction of carbon exchanges between China terrestrial ecosystem and atmosphere in 21st century. *Sci. China (Ser. D)*, **51**(6), 885–898.

Jiang, J. H., Su Hui, Zhai Chengxing, et al., 2012: Evaluation of cloud and water vapor simulations in CMIP5 climate models using NASA "A-Train" satellite observations. *J. Geophys. Res.*, **117**, doi: 10.1029/2011JD017237.

Jie Weihua and Wu Tongwen, 2010: Hindcast for the 1998 summer heavy precipitation in the Yangtze and Huaihe River valley using BCC_AGCM2.0.1 model. *Chinese J. Atmos. Sci.*, **34**(5), 962–978. (in Chinese)

—–, —–, Wang Jun, et al., 2013: Improvement of 6–15 day precipitation forecasts using a time-lagged ensemble method. *Adv. Atmos. Sci.*, **30**, doi: 10.1007/s00376-013-3037-8.

Jing Xianwen and Zhang Hua, 2012: Application and evaluation of McICA cloud-radiation framework in the AGCM of the National Climate Center. *Chinese J. Atmos. Sci.*, **36**(5), 945–958, doi: 10.3878/j.jssn.1006-9895. (in Chinese)

Li Weijing, Zhang Peiqun, Li Qingquan, et al., 2005: Research and operational application of dynamical climate model prediction system. *J. Appl. Meteor. Sci.*, **16**(Suppl.), 1–11. (in Chinese)

Li Weiping, Liu Xin, Nie Suping, et al., 2009: Comparative studies of snow cover parameterization schemes used in climate models. *Adv. Earth Sci.*, **24**(5), 512–522. (in Chinese)

Lu Chunhui, Ding Yihui, and Zhang Li, 2014: A study on numerical simulation of characteristics of stratospheric circulation changes with BCC_AGCM2.1 model. *Acta Meteor. Sinica*, doi: 10.11676/qxxb2014.006.

Luo Yong, Zhao Zongci, Xu Ying, et al., 2005: Projections of climate chang over China for the 21st century. *Acta Meteor. Sinica*, **19**(4), 400–406. (in Chinese)

Moberg, A., D. M. Sonechkin, K. Holmgren, et al., 2005: Highly variable Northern Hemisphere temperatures reconstructed from low- and high-resolution proxy data. *Nature*, **433**(7026), 613–617.

Myhre, G., B. H. Samset, M. Schulz, et al., 2012: Radiative forcing of the direct aerosol effect from AeroCom Phase II simulations. *Atmos. Chem. Phys.*, **12**, 22355–22413.

Oleson, K. W., Y. Dai, G. Bonan, et al., 2004: Technical Description of the Community Land Model (CLM), NCAR/TN-461+STR, NCAR, Boulder, Colorado, USA.

Qiao Fangli, Yuan Yeli, Yang Yongzeng, et al., 2004: Wave-induced mixing in the upper ocean: Distribution and application to a global ocean circulation model. *Geophys. Res. Lett.*, **31**, L11303, doi: 10.1029/2004GL019824.

Rasch, P. J., and J. E. Kristjánsson, 1998: A comparison of the CCM3 model climate using diagnosed and predicted condensate parameterizations. *J. Climate*, **11**, 1587–1614.

Semtner, A. J., 1976: A model for the thermodynamic growth of sea ice in numerical investigations of climate. *J. Phys. Oceanogr.*, **6**, 27–37.

Shen Zhen, Zhang Yaocun, Xiao Hui, et al., 2011: Ability of the model BCC_AGCM2.0.1 to reproduce Meiyu precipitation. *Meteor. Mon.*, **37**(11), 1336–1342. (in Chinese)

Shi Guangyu and Zhang Hua, 2007: The relationship between absorption coefficient and temperature and their effect on the atmospheric cooling rate. *J. Quant. Spectrosc. Ra.*, **105**, 459–466.

Song Zhenya, Qiao Fangli, Lei Xiaoyan, et al., 2007: The establishment of an atmosphere-wave-ocean circulation coupled numerical model and its application in the North Pacific SST simulation. *J. Hydrodyn.*, **22**, 543–548.

Su Hui, J. H. Jiang, Zhai Chengxing, et al., 2013: Diagnosis of regime-dependent cloud simulation errors in CMIP5 models using "A-Train" satellite observations and reanalysis data. *J. Geophys. Res.*, **118**, 2762–2780, doi: 10.1029/2012JD018575.

Sun Ying and Ding Yihui, 2008: An assessment on the performance of IPCC AR4 climate models in simulating interdecadal variations of the East Asian summer monsoon. *Acta Meteor. Sinica*, **22**, 472–488. (in Chinese)

Tang Guoli and Ren Guoyu, 2005: Reanalysis of surface air temperature change of the last 100 years over China. *Climatic Environ. Res.*, **10**, 791–798.

Trenberth, K. E., P. D. Jones, P. Ambenje, et al., 2007: Observations: Surface and atmospheric climate change. *Climate Change 2007: The Physical Science Basis*. Solomon, S., D. Qin, M. Manning, et al., Eds., Cambridge University Press, Cambridge, United Kingdom and New York, NY, USA.

Uppala, S. M., et al., 2005: The ERA-40 re-analysis. *Quart. J. Roy. Meteor. Soc.*, **131**, 2961–3012, doi: 10.1256/qj.04.176.

Wang Lu, Zhou Tianjun, Wu Tongwen, et al., 2009: Simulation of the leading mode of Asian Australian monsoon interannual variability with the Beijing Climate Center atmospheric general circulation model. *Acta Meteor. Sinica*, **67**(6), 973–982. (in Chinese)

Wei Xiaodong and Zhang Hua, 2011: Analysis of optical properties of nonspherical dust aerosols. *Acta Optica Sinica*, **31**(5), 0501002.

Winton, M., 2000: A reformulated three-layer sea ice model. *J. Atmos. Ocean Technol.*, **17**, 525–531.

Wu Tongwen, 2012: A mass-flux cumulus parameterization scheme for large-scale models: Description and test with observations. *Climate Dyn.*, **38**, 725–744, doi: 10.1007/s00382-011-0995-3.

—— and Wu Guoxiong, 2004: An empirical formula to compute snow cover fraction in GCMs. *Adv. Atmos. Sci.*, **21**, 529–535, doi: 10.1007/BF02915720.

——, Yu Rucong, and Zhang Fang, 2008: A modified dynamic framework for the atmospheric spectral model and its application. *J. Atmos. Sci.*, **65**, 2235–2253.

——, ——, ——, et al., 2010: The Beijing Climate Center atmospheric general circulation model: Description and its performance for the present-day climate. *Climate Dyn.*, **34**, 123–147, doi: 10.1007/s00382-008-0487-2.

——, Li Weiping, Ji Jinjun, et al., 2013: Global carbon budgets simulated by the Beijing Climate Center climate system model for the last century. *J. Geophys. Res: Atmos.*, **118**, 4326–4347, doi: 10.1002/jgrd.50320.

Xia Kun, Luo Yong, and Li Weiping, 2011: Simulation of freezing and melting of soil on the Northeast Tibetan Plateau. *Chinese Sci. Bull.*, **56**(20), 2145–2155.

Xiao Chuliang and Zhang Yaocun, 2012: The East Asian upper-tropospheric jet streams and associated transient eddy activities simulated by a climate system model BCC_CSM1.1. *Acta Meteor. Sinica*, **26**(6), 700–716.

Xie, P., and P. A. Arkin, 1997: Global precipitation: A 17-year monthly analysis based on gauge observations, satellite estimates, and numerical model outputs. *Bull. Amer. Meteor. Soc.*, **78**, 2539–2558.

Xin Xiaoge, Wu Tongwen, and Zhang Jie, 2012: Introduction of CMIP5 experiments carried out by BCC climate system model. *Adv. Climate Change Res.*, **8**, 378–382. (in Chinese)

——, Cheng Yanjie, Wang Fang, et al., 2013a: Asymmetry of surface climate change under RCP2.6 projections from the CMIP5 models. *Adv. Atmos. Sci.*, **30**, 796–805, doi: 10.1007/s00376-012-2151-3.

——, Wu Tongwen, Li Jianglong, et al., 2013b: How well does BCC_CSM1.1 reproduce the 20th century climate change over China? *Atmos. Oceanic Sci. Lett.*, **6**, 21–26.

——, ——, and Zhang Jie, 2013c: Introduction of CMIP5 experiments carried out with the climate system models of Beijing Climate Center. *Adv. Climate Change Res.*, **4**(1), 41–49.

——, Zhang Li, Zhang Jie, et al., 2013d: Climate change projections over East Asia with BCC_CSM1.1 under RCP scenarios. *J. Meteor. Soc. Japan*, **91**, 413–429.

Zhang, G. J., and N. A. McFarlane, 1995: Sensitivity of climate simulations to the parameterization of cumulus convection in the Canadian Climate Centre general circulation model. *Atmos. Ocean*, **33**, 407–446.

Zhang Hua, T. Nakajima, and Shi Guangyu, et al., 2003: An optimal approach to overlapping bands with correlated k-distribution method and its application to radiative calculations. *J. Geophys. Res.*, **108**, 4641–4654, doi: 10.1029/2002JD003358.

——, Shi Guangyu, T. Nakajima, et al., 2006a: The effects of the choice of the k-interval number on radiative calculations. *J. Quant. Spectrosc. Ra.*, **98**(1), 31–43.

——, T. Suzuki, T. Nakajima, et al., 2006b: Effects of band division on radiative calculations. *Opt. Eng.*, **45**(1), 016002, doi: 10.1117/1.2160521.

——, Wang Zhili, Wang Zaizhi, et al., 2012: Simulation of direct radiative forcing of aerosols and their effects on East Asian climate using an interactive AGCM-aerosol coupled system. *Climate Dyn.*, **38**, 1675–1693, doi: 10.1007/s00382-011-1131-0.

Zhang, L., M. Dong, and T. Wu, 2011: Changes in precipitation extremes over eastern China simulated by the Beijing Climate Center Climate System Model (BCC_CSM1.0). *Climate Res.*, **50**, 227–245.

——, Wu Tongwen, Xin Xiaoge, et al., 2012: Projections of annual mean air temperature and precipitation over the globe and in China during the 21st century by the BCC Climate System Model BCC_CSM1.0. *Acta Meteor. Sinica*, **26**(3), 362–375.

——, Wu Tongwen, Xin Xiaoge, et al., 2013: The annual modes of tropical precipitation simulated by Beijing Climate Center climate system model (BCC_CSM). *Chinese J. Atmos. Sci.*, **37**(5), 994–1012. (in Chinese)

Zhang Minhua, Lin Wuyin, C. S. Bretherton, et al., 2003: A modified formulation of fractional stratiform condensation rate in the NCAR community atmospheric model (CAM2). *J. Geophys. Res.*, **108**(D1), ACL 10-1-ACL 10-11, doi: 10.1029/2002JD002523.

Zhang Peiqun, Li Qingquan, Wang Lanning, et al., 2004: Development and application of dynamic climate model prediction system in China. *Sci. Technol. Rev.*, **7**, 17–21.

Zhao Shuyun, Zhi Xiefei, Zhang Hua, et al., 2013: A primary assessment of the simulated climatic state by a coupled aerosol-climate model BCC_AGCM2.0.1_CAM. *Climatic Environ. Res.*, doi: 10.3878/j.issn.1006-9585.2012.12015.

Zhao Zongci, Wang Shaowu, Xu Ying, et al., 2005: Attribution of the 20th century climate warming in China. *Climatic Environ. Res.*, **10**(4), 808–817. (in Chinese)

Zhou Tianjun and Yu Rucong, 2006: Twentieth-century surface air temperature over China and the globe simulated by coupled climate models. *J. Climate*, **19**, 5843–5858.

Zhou Wenyan, Luo Yong, and Li Yunmei, 2010: Validation of the radiative transfer parameterization scheme in land surface process model. *Acta Meteor. Sinica*, **68**(1), 12–18. (in Chinese)